Performance and ageing behavior of water-processed LiNi0.5Mn0.3Co0.2O2/Graphite lithium-ion cells

Marie Bichon, Dane Sotta, Eric de Vito, Willy Porcher, Bernard Lestriez

Performance and Ageing Behavior of Water-Processed $LiNi_{0.5}Mn_{0.3}Co_{0.2}O_2$/Graphite Lithium-Ion Cells

Marie Bichon[*,a], Dane Sotta[a], Eric De Vito[a], Willy Porcher[a], Bernard Lestriez[b]*

[a]Université Grenoble Alpes, CEA-Liten, 17 Avenue des Martyrs, F-38054 Grenoble, France

[b]Institut des Matériaux Jean Rouxel, UMR CNRS 6502, Université de Nantes, 2 rue de la Houssiniere, BP32229, F-44322 Nantes, France

Corresponding Author

*E-mail: marie.bichon2@gmail.com

ABSTRACT

In this study, water-processed $LiNi_{0.5}Mn_{0.3}Co_{0.2}O_2$ cathodes (NMC532) are investigated. Notably, corrosion of the aluminum current collector occurring in aqueous processing owing to the alkalinity of the NMC slurry is avoided through the addition of phosphoric acid which buffers the slurry pH, or by using a carbon-coated collector. The impact of small amounts of phosphoric acid on the electrochemical performance is evaluated in half cells, and the best formulations are selected to perform further ageing tests in pouch cells. In particular, post mortem analyses such as electrochemical impedance spectroscopy and X-ray photoelectron spectroscopy are conducted on

the cathodes after long-term cycling in Li-ion cells to fully understand the enhanced cycling stability observed with H_3PO_4-containing water-based cathode. These analyses allow to conclude on the influence of the binder, the current collector, and the aqueous immersion of the NMC532 powder.

KEYWORDS

Li-ion battery, NMC cathode, aqueous electrode processing, ageing behavior, phosphoric acid, carbon-coated collector.

1 INTRODUCTION

Lithium nickel cobalt manganese oxides (NMC) are cathode materials of interest for the implementation of high energy density lithium-ion batteries—such as in electric vehicles—as they can provide high capacity, notably with increasing nickel content. Conventionally, the manufacturing process of such NMC electrodes involves *N*-methyl pyrrolidone (NMP), as this solvent has good solubility properties regarding polyvinylidene fluoride (PVDF), which is typically used as cathode binder due to its high electrochemical stability and good mechanical properties. As NMP is a toxic solvent, removing it—typically by replacing it with water—can allow to reduce both the environmental impact and the cost of the cathode manufacturing process, due to the lower cost of water and many water soluble binders compared to NMP and PVDF[1], as well as some substantial reduction on capital and operating costs, as there is no need for solvent recovery when substituting NMP by water[2].

Yet, mixing the electrode components in water raises some challenges to obtain electrodes with comparable properties to those processed in NMP, notably because lithium transition metal oxides such as NMC material are prone to react with water. Upon contact with moisture, the surface of

NMC particles is altered, notably by the formation of LiOH and Li_2CO_3 species[3–5]. Besides, lithium leaching has been reported, sometimes along with Li^+/H^+ cation exchange reaction[4,6], and it is believed to trigger the formation of a rock-salt phase on the outer layers of the particles[6,7]. Such surface modifications are not without consequences for the electrochemical performance in a battery cell. As the rock-salt phase is not as well conductive of lithium ions as the initial layered structure[8–10], it might result in a slightly higher polarization. Additionally, the surface compounds can be involved in side reactions with the electrolyte upon cycling, which might reduce the cell capacity retention[4,11].

Besides, as LiOH and Li_2CO_3 are alkaline compounds, their dissolution in the aqueous slurry causes the pH to rise. This pH elevation to the basic range might in turn result in the corrosion of the aluminum current collector when the slurry is coated onto the foil, as the oxide passive film naturally present on the aluminum foil is only stable within the range of pH 4.5-8.5[12–14]. At more alkaline pH, the passive film is dissolved and the aluminum is locally attacked by pitting corrosion. The corrosion products may interact with the active material and also increase the electrical resistance at the electrode/collector interface[15] which is detrimental to the battery performance. There are mainly two trends emerging to overcome this problem: protecting the aluminum surface to prevent direct contact with the alkaline electrode slurry[16,17], or controlling the slurry pH by various methods[12,18–20], so that it is maintained in a range where the natural Al_2O_3 passive layer is stable.

This paper reports the evaluation of water-based formulations of NMC532 electrodes containing small amounts of phosphoric acid (0-1 wt% of the dried electrode content) and coated on bare or carbon-coated aluminum current collector. Phosphoric acid was chosen in this study over other types of acidic agents as it was demonstrated to interact at the surface of NMC particles and form phosphate compounds which seem to improve the cycling performance[18,20]. The water-based

NMC532 electrodes that exhibited the best performance in half-cells were assembled with graphite-based negative electrodes, also made with water as solvent, in pouch cells. The latter showed long term cycling, confirming that the aqueous route is viable to manufacture advanced lithium-ion batteries. The cells were analyzed along with a standard electrode processed in NMP, by electrochemical impedance spectroscopy and X-ray photoelectron spectroscopy after 300 cycles so as to investigate the impact of the formulation on the ageing mechanisms.

2 EXPERIMENTAL

Water-based NMC cathodes were prepared by mixing 95wt% NMC532 (Umicore), 2% carbon black, 2% water-soluble latex binder (Zeon) and 1% carboxymethyl cellulose (Ashland, Mw = 725 000 g/mol). In the case of the acidified formulations, phosphoric acid (Sigma-Aldrich, purity 99.99%, concentration 42.5 wt%) is added prior to the addition of NMC powder. The slurries are coated onto 20 µm thick aluminum foil (referred to as "bare Al") and onto a 15 µm thick aluminum foil covered with a 2 µm thick carbon/polymer coating (referred to as "carbon-coated aluminum" or "C-C Al"). The active material loading is set at 11.5 mg.cm^{-2}. The electrodes are pressed down to a porosity of 30%. Compositions of the different cathodes formulated are summarized in **Table 1**.

More details on electrode preparation and cell design are available in the Supplementary Information file, along with details on electrochemical testing and XPS measurements.

Table 1: Presentation of the different formulations discussed in this study.

Ref.	NMC532	CB	Binder	Solvent	H_3PO_4	Collector
F0	95%	C65 2%	PVDF 3%	NMP*	-	Bare Al
F1	95%		CMC 1%, latex 2%	Water	-	Bare Al
F1'						C-C Al
F2-a	94.9%				0.1%	Bare Al

F2'-a						C-C Al
F2-b	94.7%				0.3%	Bare Al
F2'-b						C-C Al
F2-c	94.5%				0.5%	Bare Al
F2'-c						C-C Al
F2-d	94%				1%	Bare Al
F2'-d						C-C Al

Sigma-Aldrich, anhydrous, 99,5%

3 RESULTS

3.1 Performance evaluation in coin cells

The electrochemical performance of the cathode formulations presented in **Table 1** was evaluated in coin cell, using a lithium metal anode (Sigma-Aldrich, 99.99% purity, 60 µm thick, disc of 16 mm diameter). For each formulation, three coin cells were prepared and the capacity plots displayed below correspond to the average capacity of these three cells. The standard error is calculated for each averaged capacity value and is represented through the pale halo surrounding the capacity curves.

3.1.1 Performance of water-based formulation F1 and F1' using bare or carbon-coated aluminum current collector

The **Figure 1.a** displays the averaged cycling behavior of the water-based formulations coated on bare (F1) and C-C Al collector (F1'). The use of the carbon coating is to prevent direct contact between the alkaline aqueous slurry and the aluminum surface, so as to avoid corrosion of the latter. In practice, as the carbon layer is porous, corrosion cannot be completely inhibited but it still is efficient to limit the extent of aluminum corrosion. The carbon-coated aluminum collector results in an improved capacity retention as well as reduced cell-to-cell variation. Indeed, for the electrodes F1 subjected to aluminum corrosion, the cell-to-cell variation increases during the cycling test, and is much larger after 200 cycles compared to the corrosion-free electrodes F1'. As the aluminum

foil is not uniformly corroded, but rather locally, it is not surprising to observe a large cell-to-cell variation for the formulation F1, as the extent of corrosion might vary from one cell to the other. The observation of pits in the electrode surface due to H_2 release is sign of aluminum corrosion, which was observed for F1 but not for F1'(**Figure S2**). The higher capacity fade exhibited by the electrodes F1 compared to F1' is accounted for by a faster impedance buildup upon cycling (**Figure S3**).

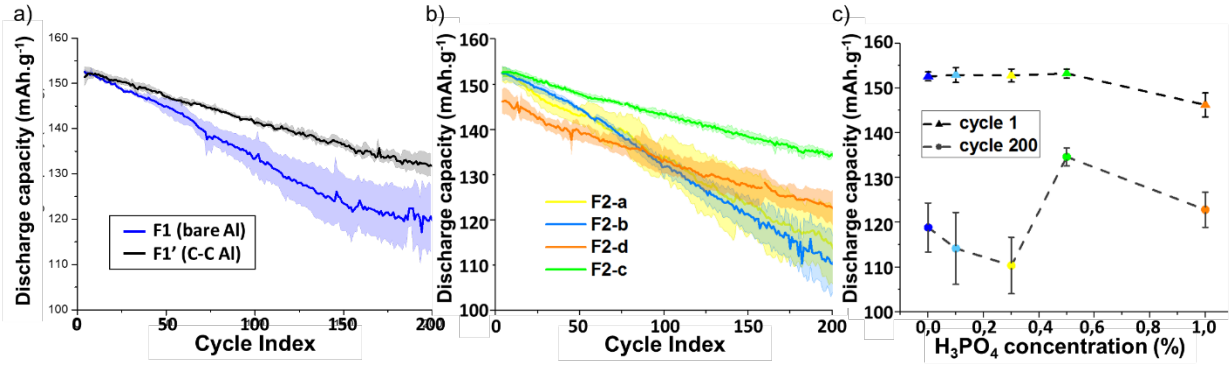

Figure 1: Average capacity retention of water-based electrodes vs lithium in coin cells **a)** acid-free formulations F1 and F1', and **b)** H_3PO_4-containing formulations F2. **c)** Capacity of the 1st and 200th cycles plotted as a function of H_3PO_4 content (the formulation with 0% H_3PO_4 corresponds to F1).

3.1.2 Impact of H_3PO_4 concentration on the cycling behavior of aqueous formulations F2

The capacity plots of the formulations F2-a, F2-b, F2-c and F2-d—which contain respectively 0.1%, 0.3%, 0.5% and 1% of phosphoric acid—are displayed in **Figure 1.b**. The amount of phosphoric acid seems to affect the cycling performance, as the formulations F2 exhibit distinct cycling behaviors. Yet, this relationship is not linear, as evidenced on the **Figure 1.c**, which presents the initial and final capacities at 0.5C for the four formulations, depending on the H_3PO_4 content. In fact, the best performance is achieved with the formulation F2-c containing 0.5% H_3PO_4. As discussed in a previous article[20], the addition of phosphoric acid in the aqueous slurry results in surface degradation of NMC particles as well as formation of phosphate compounds.

Lithium leaching, induced structural change and formation of insulating species such as Li_2CO_3, that are exacerbated in acidic medium, are believed to increase the cell polarization, resulting in lower initial capacity. To verify this assumption, the amount of protons introduced in the aqueous slurry of each formulation—through the addition of H_3PO_4—was calculated, and the initial charge and discharge capacities were plotted as a function of this proton content in **Figure S4**. The results highlight the fact that, indeed, the initial charge and discharge capacities tend to decrease with the slurry acidity.

However, the phosphate compounds at the surface of the NMC particles seem to enhance the cycling stability. From the results presented in **Figure 1.b**, it appears that a concentration of 0.5% H_3PO_4 offers a good compromise between enhanced stability and low impact on the initial capacity impact. With 1% H_3PO_4 (formulation F2-d), the capacity decay per cycle seems to be as low as with 0.5% H_3PO_4, yet the discharge capacity delivered is much lower. The poor specific capacity obtained with the formulation F2-d might also be related to the fact that the electrodes exhibited very weak adhesion properties regarding the aluminum collector. The cycling behavior of the water-based formulations containing 0.1% H_3PO_4 (F2-a) and 0.3% H_3PO_4 (F2-b) is similar to what was obtained with the acid-free formulation F1, as presented in **Figure 1.a**. Indeed, the cell-to-cell variation also increases upon cycling, and on average the cells exhibit similar capacity decay. The composition of the F2-a electrodes is actually very close to F1, as the small amount of phosphoric acid (0.1%) is insufficient to inhibit the aluminum corrosion. With 0.3% H_3PO_4, no signs of collector corrosion were observed (**Figure S2**), yet this does not improve the cycling stability. In this case the addition of phosphoric acid might be more harmful to the cycling performance as the amount of phosphate compounds is not sufficient to efficiently protect the active material from further degradation upon contact with the electrolyte (e.g. material dissolution).

As the carbon-coated collector tested with the non-acidified aqueous formulation (F1') led to enhanced electrochemical performance compared to bare aluminum (F1), the application of such coated collector was also considered for the acidified formulations F2, although it is not necessary when the amount of H_3PO_4 is enough to mitigate the aluminum corrosion. However, the formulations F2'-a, F2'-b and F2'c coated onto C-C Al collector did not exhibit better cycling performance than the formulations F2-a, F2-b and F2-c coated onto bare aluminum (**Figure S5**).

3.2 Performance evaluation and study of the ageing behavior in pouch cells

In the wake of the study in half-cells presented above, the formulations with the best cycling performance (i.e. F0, F1' and F2-c, as shown in **Figure 2.a**) were selected to perform further ageing tests. For this purpose, new electrode tapes were prepared and cut to be assembled in pouch cells against a graphite anode. With this cell design, the cycle life is significantly extended when graphite is used instead of lithium metal at the anode. Three pouch cells were prepared for each formulation. After 300 cycles, one out of the three was stopped to perform post mortem analyses, so only two cells per formulation remained cycling. To evaluate the ageing behavior of the formulations, comparison is drawn between some cycles selected at different timeframe of the cycling test, so that the following different stages are investigated: at the beginning (cycle 30), in correspondence with the post mortem analyses (cycle 330), and after extensive cycling (cycle 1030).

3.2.1 Cycling stability

The capacity plot of the pouch cells cycled for more than 1000 cycles is presented in **Figure 2.b**. The cells are charged at 0.5C and discharged at 1C, and a rate performance test (charge at 0.5C, and discharge from 0.1C to 5C) is applied every 100 cycles. However, only the data points corresponding to the discharge rate of 1C are displayed in **Figure 2.b**, so as to make the graph reading easier. Although the cycling conditions applied to the pouch cells are different from the

coin cells (which are charged at 0.2C and discharged at 0.5C), the same trend is observed in **Figure 2.a** and **Figure 2.b**. The organic formulation F0 initially delivers the highest capacity while the aqueous formulation F2-c delivers the lowest initial capacity. Yet, the former and latter formulations exhibit respectively the poorer and better capacity retention, so that after hundreds of cycles, the capacity delivered by the three formulations range in the following order: F2-c > F1' > F0. Generally, the capacity fade presented in Figure 2.b is important compared to other studies, especially for NMP-based slurries[21–23]. The capacity retention is much higher in coin cells (Figure 2.a), with 83%, 93% and 94% after 200 cycles respectively for F0, F1' and F2-c. The protocol for SEI formation on graphite anode could be improved to avoid fast capacity decay with the pouch cells. Nevertheless, the performance of the three formulations can still be compared in this study.

In the **Figure 2.b**, although only the data points corresponding to a discharge rate of 1C are displayed, a small capacity recovery is observed every 100 cycles (the charge current density is always 0.5C). This capacity fluctuation that occurs after the rate performance test can be attributed to the trapping of active lithium in the anode at high rate, which can be inserted back in the NMC at slow rate (see **Figure S7** and the text in SI for more details).

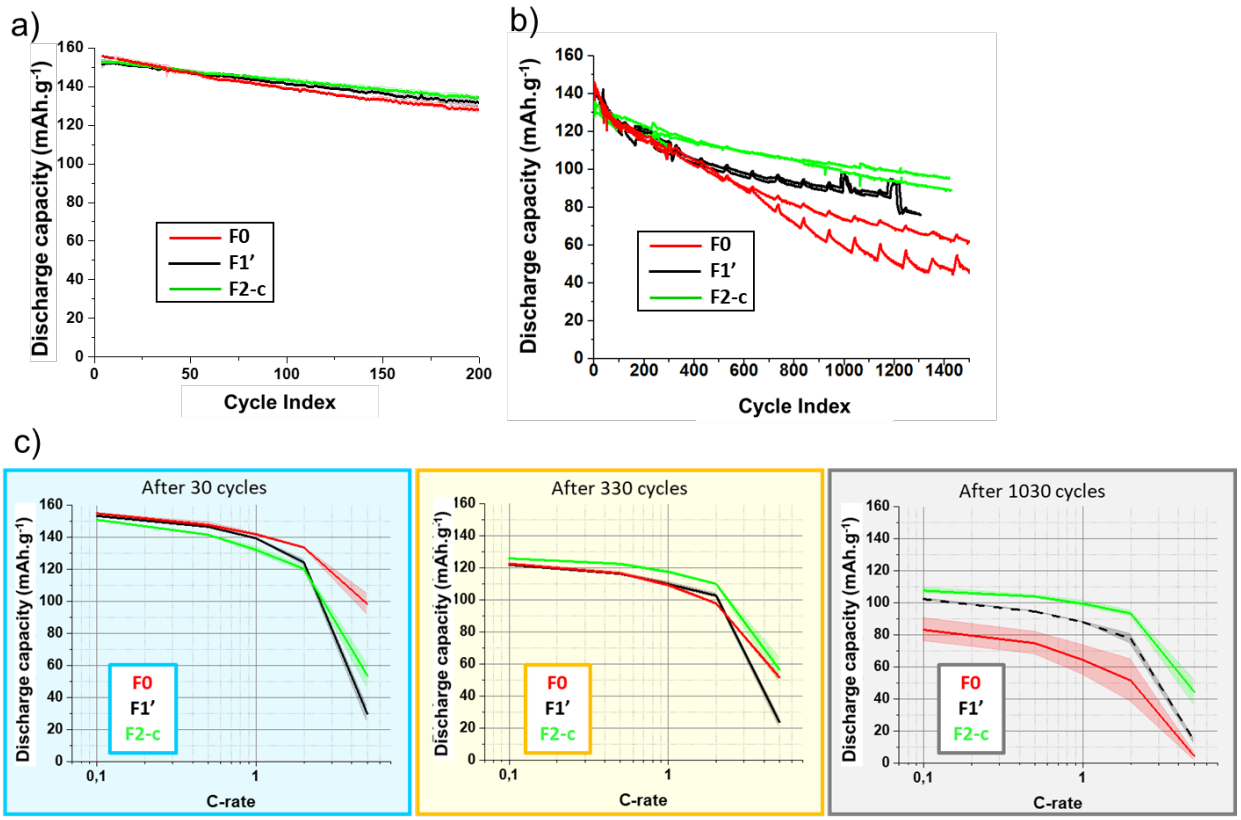

Figure 2: Cycling performance of the formulations F0, F1' and F2-c **a)** in half cells, discharged at 0.5C, and **b)** in full cells, discharged at 1C. **c)** Comparison of the rate performance of the three formulations evaluated after 30, 330 and 1030 cycles.

3.2.2 Rate capability

The rate performance tests performed every 100 cycles are presented in **Figure S8,** which displays the average capacity obtained at each discharge rate as the test consists of a series of three cycles charged at 0.5C and discharged successively at 1C, 0.1C, 0.5C, 2C and 5C (15 cycles in total). In **Figure 2.c**, the rate capability tests performed after 30 cycles, 330 cycles and 1030 cycles are plotted for each formulation (it corresponds to the data circled in color in **Figure S8**).

In the first rate capability test (after 30 cycles), the organic formulation F0 delivers the highest capacity at all C-rates. Similar performance is obtained with the aqueous formulation F1' up to 1C,

but at higher rate—especially 5C—the capacity is substantially decreased. On the other hand, the formulation F2-c delivers slightly lower capacity than F0 and F1' at low and intermediate C-rate, but it outperforms the aqueous formulation F1' at 5C.

At low C-rate (<1C), the capacity is mostly limited by the electrode resistance (contact electrode/collector, CB percolation, SEI and CEI layer and charge transfer resistance)[24] while at high C-rate (>2C for the active mass loadings studied here), the rate capacity is limited by diffusion of lithium salt across the electrode through its porosity. Here, the influence of the graphite anode on the discharge capacity at high C-rate cannot be neglected. In other words, the NMC cathode is not necessarily the limiting electrode at high discharge currents in full cells. Mao et al.[25] studied the rate limiting factors for fast charging in NMC811/graphite cells. They concluded from rate capability tests in half-cells that the lithiation of the graphite anode was the limiting step in fast charges above 3C, owing to longer (more tortuous) lithium-ion transport distance in the electrolyte and salt depletion inside the graphite electrode thickness. Given that the areal capacity of the graphite electrodes in this work is lower than in the study by Mao et al. (2.1 $mAh.cm^{-2}$ vs 2.6 $mAh.cm^{-2}$), it means that the electrodes thickness is also lower, which implies less mass transport limitations for the graphite electrodes in this work. Thus, it can be assumed that, here, the NMC532 cathode is the limiting electrode at least up to 2C.

We can conclude from the rate performance tests after 30 cycles that the electrode morphology obtained with PVDF binder (F0) seems to induce less electrode resistance compared to CMC-based electrodes F1' and F2-c, as it leads to higher capacity at high C-rate[26]. This might be related to the morphology of the electrodes, as it appears in fact that a higher percentage of the NMC surface area is covered by the water-based CMC/latex binders compared to PVDF (see **Figure S9**). This coverage might hinder fast lithium transfer, which is a limiting factor at high rate[24]. Regarding the

electrode F2-c, the lower capacity obtained below 1C compared to the other formulations in the initial rate capability test could be ascribed to a higher electronic resistance due to the phosphate compounds on the active material surface. When it comes to comparing the performance at 5C of the water-based formulations F1' and F2-c, several hypotheses can be drawn. First, if the cathode is assumed to be the limiting electrode, the higher capacity obtained with F2-c could be related to the addition of H_3PO_4 in the formulation (a decreased amount of insulating Li_2CO_3 compounds and formation of good ionic conductor Li_3PO_4 is believed to facilitate fast lithium diffusion[27,28]). Then, if the graphite anode is assumed to be the limiting electrode, there still might be an effect of the cathode (migration of species from the cathode and deposition at the anode) that accounts for the discrepancy observed at 5C between the two aqueous formulations F1' and F2-c. For instance, it could be proposed that the precipitation of phosphate compounds on the F2-c electrode act as a coating by limiting the dissolution of transition metals and deposition at the anode. Or, it can also be suggested that the use of the carbon-coated collector is somehow responsible for the poor performance of graphite anode at 5C, through the release or dissolution of species from the carbon coating in the electrolyte, that then interact with the anode. These hypotheses are further discussed in the SI (**Figures S10-11**).

The trend described above regarding the first rate performance test conducted after 30 cycles is however not maintained in the following rate capacity tests. Indeed, as F0 undergoes a fast capacity decay over cycling, its rate performance is quickly lessened, while the formulation F2-c which exhibits the best capacity retention eventually displays also the best performance at all C-rates in the following tests.

3.3 Analysis of capacity fade mechanisms

The mechanisms of capacity fade occurring to the three main formulations F0, F1' and F2-c are investigated more closely in this section. The increase of polarization is first examined by considering the evolution of the internal resistance and through the voltage profiles and differential capacity curves plotted for some selected cycles (30, 330, and 1030). Additional information regarding the impedance contributions is obtained by electrochemical impedance spectroscopy. Then, the mechanisms responsible for capacity loss are investigated through differential voltage analysis and XPS characterizations.

3.3.1 Impedance buildup

The voltage profiles and differential capacity plots corresponding to the 30^{th}, 330^{th} and 1030^{th} cycles of F0, F1' and F2-c are displayed in **Figure 3.a-b**. In the differential capacity plots, the anodic/cathodic peaks of the electrode F0 are progressively shifted towards higher/lower potentials upon cycling, which reveals that the capacity decay is due to a significant impedance increase. The same phenomenon is also observed with the electrode F1', albeit to a lesser extent. Interestingly, it seems that the polarization with F0 is higher upon discharge rather than during the charge, as evidenced in the voltage profiles after 330 and 1030 cycles. In case of the electrode F2-c, which exhibits the highest capacity retention, the anodic and cathodic peaks are barely shifted after 1030 cycles in the differential capacity plots, indicating that the cell resistance is rather constant.

These results are in good agreement with the internal resistance measurements that are performed at mid-charge (3.7V) every 10 cycles, and are displayed in **Figure S12**. This latter graph reveals that indeed, the internal resistance of the F0 cells increases drastically upon cycling (it is multiplied by a factor 5 after 1200 cycles), while only a slight increase of the internal resistance is observed for the F1' cells (which is doubled after 1200 cycles), and the internal resistance remains

rather constant for the F2-c cells. Note that the higher polarization of the formulation F2-c observed on the differential capacity plots at the 30th cycle is correlated to a slightly higher internal resistance measured initially. As the cells internal resistance is measured during a 20 s discharge pulse after a 30 min rest, it includes mainly the ohmic and charge transfer resistance while diffusion is hardly included[29]. More information on the contribution of these different resistances can be obtained using electrochemical impedance spectroscopy.

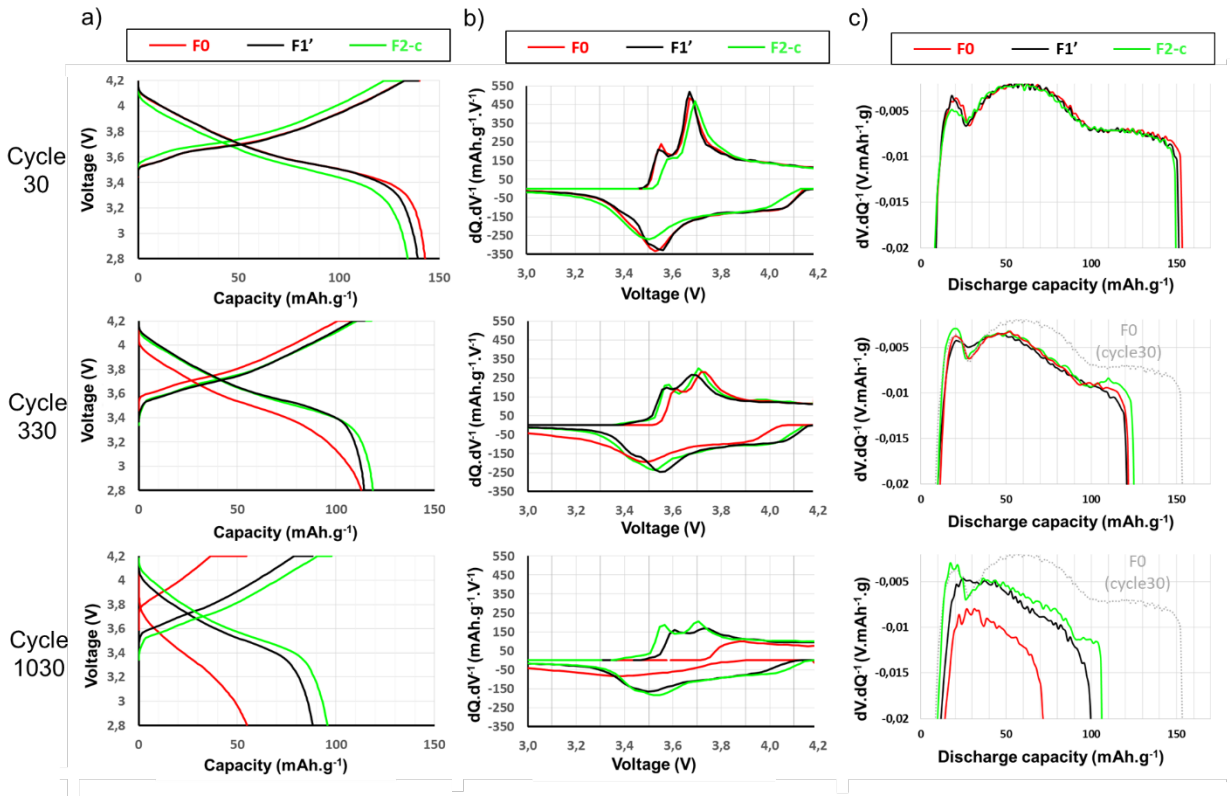

Figure 3: **a)** Voltage profiles, **b)** differential capacity curves, and **c)** differential voltage curves of the full cells F0, F1' and F2-c, plotted for the cycles 30, 330 and 1030.

The Nyquist plots of the symmetrical coin cells assembled from NMC cathodes and graphite anodes recovered from the pouch cells after 2 or 300 cycles are shown in **Figure 4**. For both electrodes, the Nyquist plot is generally composed of two depressed semicircles at high to medium frequencies, followed by a slope in the low-frequency range. The equivalent circuit used to fit the

Nyquist plot is displayed in **Figure S13**. At high frequency, the intercept of the semicircle with the real axis corresponds to the sum of the ohmic resistances of the electrolyte and other cell components (R_1). The loop at high frequency (~1 kHz) describes the response of various electrochemical processes; it generally characterizes the resistance of the SEI film on the graphite anode[10,30–32]. However, for the NMC cathodes, as surface films are much thinner, their resistance is not predominant in this frequency range. In fact, as electrochemical processes are dependent on the temperature contrary to electronic phenomena, impedance measurements at 0°C and 25°C have been carried out to confirm that the semi-circle described by the resistance R2 corresponds to the resistance of surface film for the graphite anode, and contact resistance for the NMC cathode. The high frequency loop is rather assigned to the electronic resistance of the electrodes (particle-to-particle and particle-to-collector)[10,30,33,34]. This semicircle is modeled by a resistance R_2 in parallel with a constant phase element Q_2. The loop at mid frequency (~10-100 Hz) is typically ascribed to the charge transfer resistance at the electrode material surface (R_3), with Q_3 being the capacitance of the active material double-layer. Finally, the Warburg impedance (W_4) at low frequency (<1 Hz) is related to lithium diffusion in the material or electrode bulk.

As the coin cells used for the impedance measurements are made from fresh components apart from the aged electrodes (new electrolyte, separator), the resistance R_1 has little interest in this study as it only reflects the resistance of the electrolyte and electronic wiring of the cell. Experimentally, some cells exhibited large value for the resistance R_1, probably due to some default in the cell electronic wiring, but this resistance is not shown in the Nyquist plots to make the graph reading easier (all curves are manually aligned to the same abscissa value).

The values of R_2 and R_3 obtained from the impedance data fitting are reported in **Table 2**. The impedance data are plotted according to the electrode surface (in $\Omega.cm^2$). As the working and

counter electrodes are identical, both signals overlap, and the resulting impedance is the sum of the signal of the two electrodes. The values of the resistances R_2 and R_3 given in **Table 2** are thus calculated for one electrode. Note that, in practice, if there is a slight geometrical asymmetry between the two identical electrodes, the resulting impedance measured might be slightly either underestimated or overestimated[35]. Yet the variations of the resistance that are discussed below are substantial and cannot be accounted for by a misalignment between the working and counter electrodes in the coin cell.

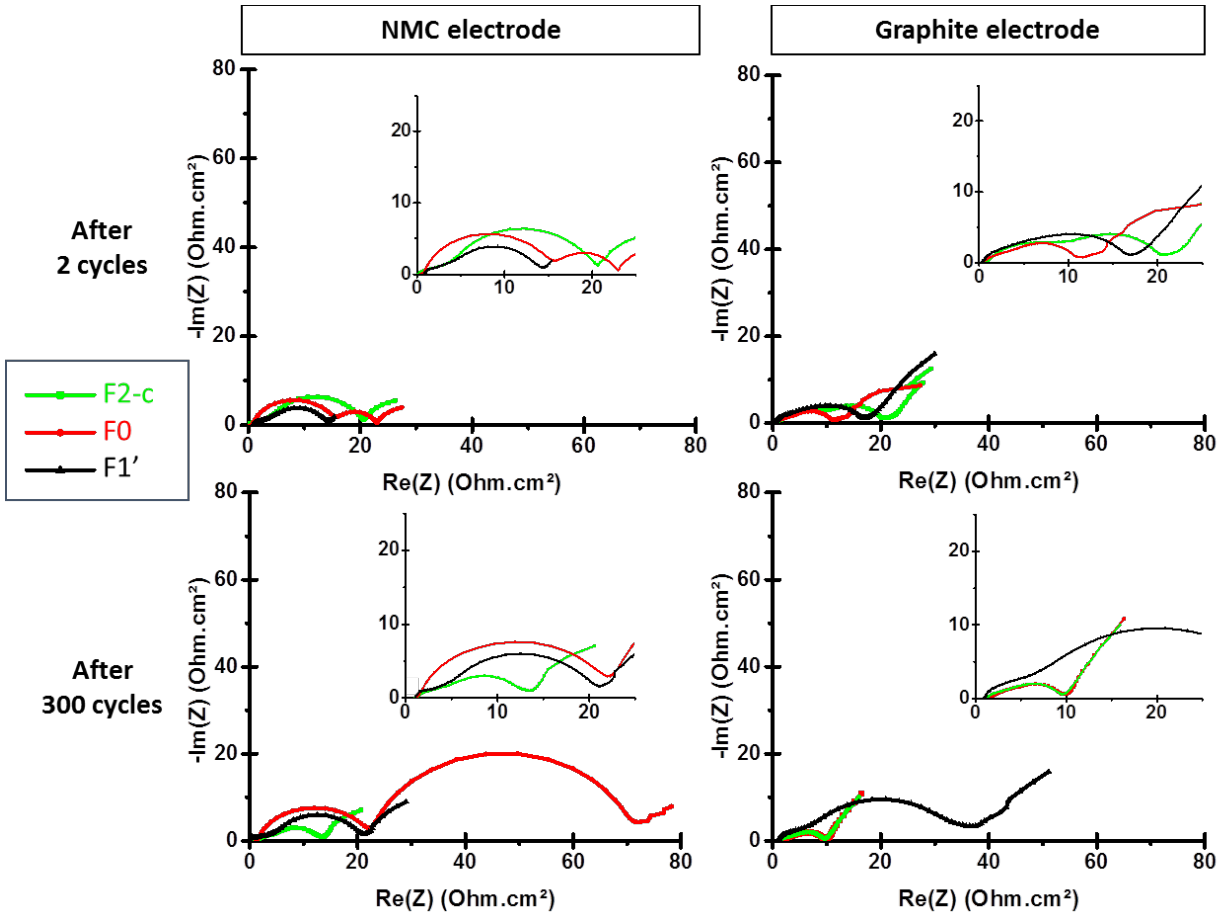

Figure 4: Nyquist plots recorded in symmetrical cells containing graphite or NMC electrode harvested from the pouch cells F0, F1' and F2-c after 2 formation cycles or after 300 cycles. A close-up of each graph is displayed in the insert figures.

Regarding the NMC electrodes, it appears clearly that the ageing behavior of the electrode F0 is different from the water-based electrodes F1' and F2-c. Indeed, the charge transfer resistance R_3 increases dramatically after 300 cycles for F0 (from 7 to 48 Ω.cm², along with a decrease of the characteristic frequency from 10 to 1 Hz) compared to the water-based cathodes. This resistance only slightly increases for F1' (from 9 to 13 Ω.cm²) while it was quite high initially for F2-c but decreases after 300 cycles (from 16 to 9 Ω.cm²). The impedance contribution ascribed to the contact resistance (R_2) follows the evolution of the charge transfer resistance (R_3), as it increases from 15 to 21 Ω.cm² for F0 while it is much lower for the water-based formulations even after 300 cycles (< 9 Ω.cm²).

Table 2: Values of the resistances R_2 and R_3, and corresponding characteristic frequencies f_2 and f_3 obtained after fitting the curves displayed in **Figure 4**.

	NMC		Graphite	
	R_2(Ω.cm²)/f_2(kHz)	R_3(Ω.cm²)/f_3(Hz)	R_2(Ω.cm²)/f_2(kHz)	R_3(Ω.cm²)/f_3(Hz)
F0 (after 2 cycles)	15 / 4	7 / 10	3 / 5	8 /80
F0 (after 300 cycles)	21 / 3	**48** / 1	3 / 6	5 / 100
F1' (after 2 cycles)	5 / 4	9 / 15	4 / 5	13 / 140
F1' (after 300 cycles)	9 / 3	13 / 10	5 / 3	**28** / 30
F2-c (after 2 cycles)	4 / 2	16 / 10	4 / 7	11 / 100
F2-c (after 300 cycles)	3 / 5	9 / 30	2 / 5	7 / 100

The impedance contribution of the graphite electrodes is very different from the matched NMC cathodes. Initially, the resistances R_2 and R_3 are quite low for all graphite electrodes, with F0 having the lowest charge transfer resistance. After 300 cycles, the charge transfer resistance of F1' is practically doubled (from 13 to 28 Ω.cm²) while R_2 and R_3 are slightly decreased for F0 and F2-c. The latter decline could be related to an increase of the graphite surface exposed to the electrolyte (access to additional pores due to improved wettability for instance).

These results indicate that the large polarization growth and resulting capacity fade reported for F0 are related to the increase of the cathode charge transfer resistance (R_3) and loss of electronic

contacts (R_2) in the NMC electrode, while in case of the formulation F1', it seems that the impedance buildup mainly originates from the increase of the charge transfer resistance at the graphite anode. Such a phenomenon might result from the release/dissolution of some species from the coating of the collector or from the NMC material (unprotected by phosphate compounds) into the electrolyte and the reaction of such species at the negative side. Regarding F0 cathode, the increased charge transfer resistance could be related to phase transformation of the NMC particle surface into spinel or rock salt structure upon cycling, as the aforementioned structures are not as well conductive of lithium ions as the initial layered structure[8–10]. Besides, degradation of the electrical conductivity of the PVDF/carbon domains upon cycling could also account for the increased electrical resistance in F0 cathode[36].

3.3.2 Capacity loss

As the analysis of voltage profiles and differential capacity curves does not allow to differentiate the ageing behavior of the cathode from the anode if a third reference electrode is not used to monitor the potential of both electrodes independently, an alternative approach is thus to consider the differential voltage plots dV/dQ as a function of the capacity. The differential voltages of the three formulations plotted for the cycles 30, 330 and 1030 are displayed in **Figure 3.c**. Comparing the evolution of these curves allows to draw qualitative conclusions regarding the origin of capacity fade.

In the differential voltage curves plotted after 30 cycles**,** the two downward peaks correspond to the transition regions between two plateaus of the graphite voltage profile (see **Figure S14** for more information). After 330 cycles, both peaks height is reduced for F1'. This feature is symptomatic of a poor homogeneity of lithium distribution (HLD) among the particles in the graphite electrode, as it highlights the fact that the transition between two voltage plateaus is no more a step function

but is rather spread out[29,37]. In case of the cell with F0, the two peaks can still be identified on the differential capacity curve after 330 cycles. Yet, it is noted that the position of the second downward peak is shifted from 100 to 95 $mAh.g^{-1}$. Such horizontal compression of the differential voltage curve reveals some loss of active material at the anode, corresponding to ~5 $mAh.g^{-1}$. The other mechanisms accounting for the capacity loss after 330 cycles include loss of active material at the cathode and consumption of lithium in the SEI (lithium inventory loss). Although these two mechanisms can be hardly told apart in a quantitative way without the use of a third electrode monitoring the individual potential of both electrodes, here it is assumed that the main contribution to capacity losses comes from lithium consumption in side reactions, as demonstrated in other studies on NMC532 / graphite cells cycled at even higher cut-off potential[21,38,39].

After 1030 cycles, the differential voltage plots of the three cells have evolved in much different directions, while they were still quite similar after 330 cycles. Following the position of the two downward peaks for F2-c, a capacity loss of ~9 $mAh.g^{-1}$ can be ascribed to the loss of active material at the graphite anode. Yet, similar conclusion cannot be drawn from the differential voltage plots of F0 and F1' as the two downwards peaks have disappeared from both curves. Again, this is related to a decrease of HLD in the graphite electrode. In case of F0 though, the primary cause of the absence of the first downward peak might be rather related to electrode slippage (see **Figure S15**); as the amount of active lithium is substantially decreased after 1030 cycles (reduction of the capacity), the graphite electrode is only partially lithiated and the lowest voltage plateau is no more reached. The phenomenon of electrode slippage—resulting from the loss of active lithium in the SEI—is also evidenced through the downward shift of the differential voltage plots. The extent of electrode slippage is more pronounced for F0 after 1030 cycles than for the aqueous formulations F2-c and F1'. This can by the way account for the higher degradation of cathode

material observed from EIS measurements for F0, as cycling of NMC electrodes at higher state of charge accelerates secondary particles cracking and phase transformation at the surface of the primary particles, which results in impedance growth[9,21]. Besides, because of electrode slippage, the potential of the graphite anode can be potentially raised at ~1.3V at the end of discharge, and the SEI may be degraded. Re-formation of SEI during cycling could also contribute to capacity loss.

3.3.3 XPS analysis of aged cathodes

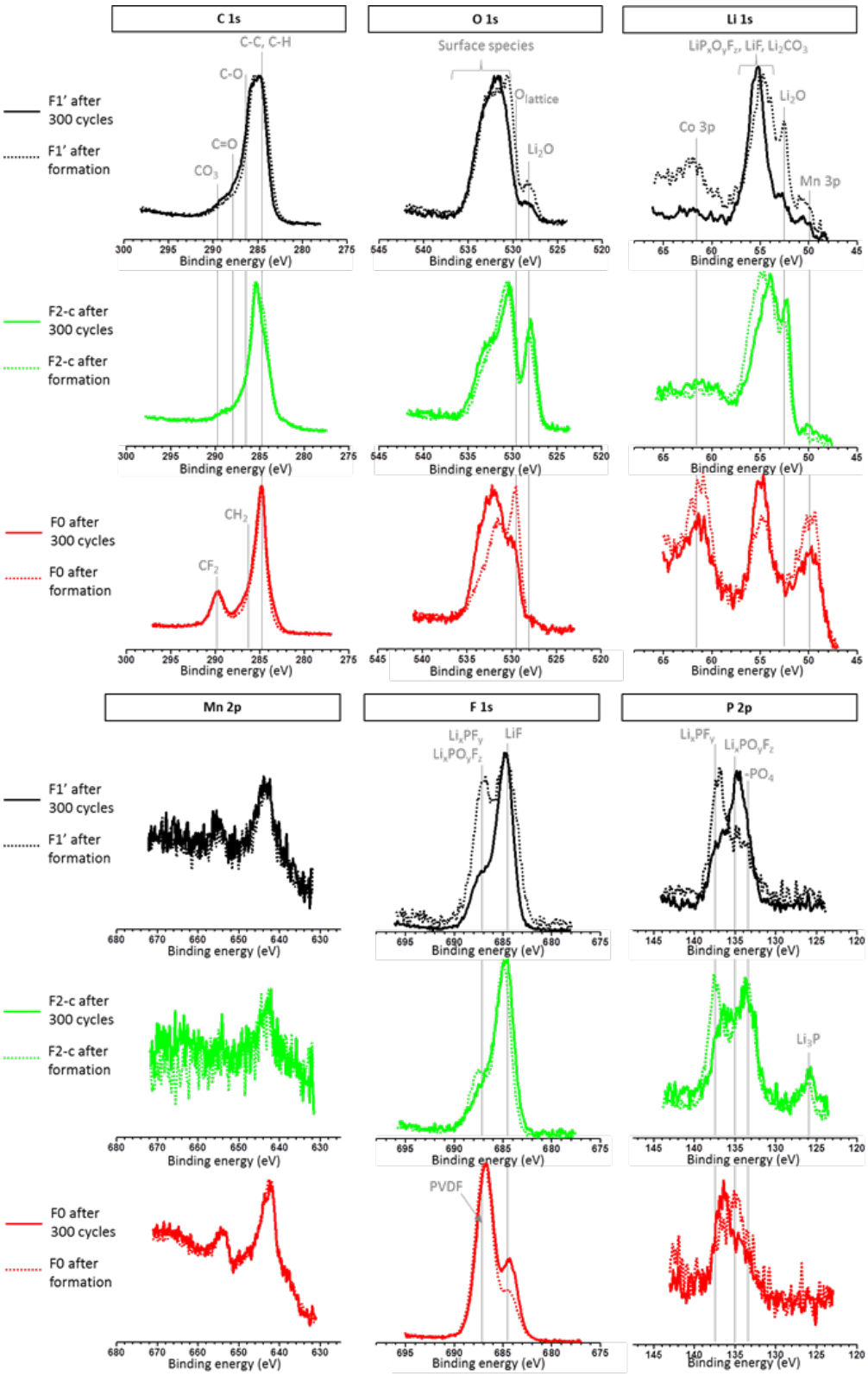

Figure 5: XPS spectra of cathodes F0, F1' and F2-c after 2 or 300 cycles. The intensity is normalized and expressed in arbitrary unit.

To obtain more information regarding the surface modification of the electrodes upon ageing, XPS analysis was performed on F0, F1' and F2-c NMC electrodes after 2 and 300 cycles. The resulting spectra are displayed in **Figure 5**, and the atomic ratio of C, O, Mn, Li, F and P—which are calculated for each electrode from the peak surface areas, and corrected by the Scofield Relative Sensitivity Factors—are reported in **Figure S16**.

Initially, the pristine electrodes contain only NMC, carbon black and binder. In the electrodes analyzed after 2 and 300 cycles, the presence of carbon black and binder can be identified despite the cathode electrolyte interphase layer (CEI) formed at the surface of the electrodes. Carbon black particles contribute mainly to the C-C/C-H peak in the C 1s spectrum. CH_2 and CF_2 groups in PVDF binder are revealed in the lines at 286.2 and 290 eV respectively for the electrode F0[40,41]. The latter functional group also contributes to the peak near 687.2 eV in the F 1s spectrum[40,41]. In the water-based electrodes F1' and F2-c, the binders are composed of 1wt% Na-CMC and 2wt% latex with acrylic functions. These polymers contribute mainly to the C-O line (and to a much lesser extent to the C=O peak) in the C 1s spectrum[42–44]. The different contributions in the O 1s spectrum have not been resolved though, as many different species have similar binding energies. In the water-based electrodes F1' and F2-c, the signal intensities from the NMC material are extensively decreased (even after 2 cycles) compared to electrode F0: this is emphasized by the smaller intensity of the Co 3p and Mn 3p peaks next to the lithium peak in the Li 1s spectra, as well as the peak near 529.5 eV ascribed to lattice oxygen in the NMC bulk, in the O 1s spectra. This feature is in fact not surprising considering the SEM pictures of the pristine electrodes in

Figure S9, wherein the NMC surface area covered by the carbon/binder phase is much larger in the aqueous processed electrodes compared to the PVDF-based electrode.

After two formation cycles, a surface layer is formed at the surface of all the electrodes. Indeed, some elements contained in the electrolyte but absent from the pristine electrodes are found at the surface of the electrodes after 2 cycles. For instance: P for F0 and F1' (not for F2-c as it initially contains phosphates, although in very small amounts, as only 0.5wt% of phosphoric acid is added to the electrode slurry per weight of NMC) or F for F2-c and F1'. This CEI layer formed after 2 formation cycles is thicker for F2-c > F1' > F0, as revealed by the more pronounced attenuation of the signals from the transition metals (Co 3p and Mn 3p) in the Li 1s spectra, compared to the intensity of the lithium peak. This observation is in line with the impedance measurements after 2 cycles; a higher charge transfer resistance was measured for F2-c compared to F1' and F0 (F2-c > F1' > F0).

After 300 cycles, it seems that the CEI thickness increases for the electrodes F0 and F1', but not for the electrode F2-c. Indeed, the elemental ratios F/Mn, P/Mn and Li/Mn are higher after 300 cycles than after 2 formation cycles for the electrodes F0 and F1', while an opposite trend is observed for the electrode F2-c (see **Table 3**). Such observation could be related to the phosphate compounds present on the pristine electrode F2-c that protect the surface from electrolyte decomposition. This trend is also in accordance with the evolution of the charge transfer resistance after 300 cycles (which increases for F0 and F1' but decreases for F2-c).

Table 3: Elemental ratios calculated from the atomic concentrations given in **Figure S16**.

	F0		F1'		F2-c	
	2 cycles	300 cycles	2 cycles	300 cycles	2 cycles	300 cycles
Ratio F/Mn	20	16	16	43	79	31
Ratio P/Mn	0.5	2.1	2.1	5.3	13.6	3.6

Ratio Li/Mn	4	35	35	58	176	103

Regarding the nature of the CEI layer formed on the electrodes upon cycling, it is interesting to compare the XPS spectra (**Figure 5**) of a same electrode after 2 and 300 cycles, but also between the different electrodes. In general, the XPS spectra of the water-based electrodes F2-c and F1' are quite similar (meaning the same species are found in both electrodes, although not in the same proportion), while more significant differences are observed in the XPS spectra of the F0 electrode. Such differences in the C 1s, O 1s and F 1s spectra originate from the electrode binder (PVDF vs CMC/latex). However, some discrepancies between the XPS spectra of all three electrodes are noteworthy to highlight. In the O 1s spectra, the photoemission line near 528.2 eV is ascribed to Li_2O. This species is found even after the formation cycles on the water-based electrodes F1' and F2-c, but not on the electrode F0. Besides, it is noted that a lower amount is observed on F1' compared to F2-c, especially after 300 cycles, indicating that Li_2O on the former electrode has been overlaid with other CEI species after 300 cycles. This result is confirmed on the Li 1s spectra, considering the peak near 52.5 eV also assigned to Li_2O. The other CEI species formed upon cycling are mainly decomposition products of the electrolyte salt, $LiPF_6$. Indeed, the C 1s spectra of all three electrodes are barely changed between 2 and 300 cycles, indicating no significant electrolyte solvent decomposition. In contrast, evolution of the F 1s and P 2p spectra after 300 cycles is related to the formation of LiF, Li_xPF_y, and $Li_xPO_yF_z$ compounds[40,45]. Regarding the P 2p spectra, it seems that after 300 cycles, the amount of fluorophosphates increases compared to the amount of Li_xPF_y for the water-based electrodes, while an opposite trend is observed for F0. Note that the highest amount of phosphate compounds is found on the electrode F2-c after the formation cycles as well as after 300 cycles. Besides, this electrode also contains trilithium phosphide at its surface, while this species is not found on F0 nor F1'. Its presence is thus likely related to the

addition of phosphoric acid in the electrode F2-c, so it is probably formed through a reaction of the electrolyte with the phosphate compounds present at the surface of the active material in the pristine electrode. Indeed, it seems reasonable to assume that Li_3P is part of the CEI formed during the formation cycles, and is not present on the pristine electrode, as this compound readily reacts in air[46], and the electrodes were exposed to ambient air before cell assembly. Moreover, no trace of Li_3P were found neither in the P 2p spectrum of NMC532 powder exposed to acidified water presented in a previous article[20]. Li_3P is known to be a good ionic conductor[47,48], and may also contribute to the lower impedance of F2-c electrodes. In the F 1s spectra, the intensity of the peak assigned to LiF increases after 300 cycles compared to the other components, for all electrodes. However, in case of the electrode F2-c, this feature is not associated with further formation of LiF, but rather with the relative reduction of the amount of Li_xPF_y and $Li_xPO_yF_z$ compounds, as the ratio F/Mn—which can be considered as representative of the evolution of the CEI layer thickness—decreases after 300 cycles for F2-c.

4 DISCUSSION

The evaluation of the electrochemical performance in half cells of the various formulations presented in **Table 1** has led to the identification of three formulations that demonstrated the best performance: a standard NMP-based formulation (F0), and two water-based formulations (F1' and F2-c). These aqueous formulations were "optimized" compared to the reference aqueous formulation F1, in the sense that corrosion of the aluminum current collector was avoided by adding 0.5% H_3PO_4 in the electrode slurry (F2-c), or using a carbon-coated collector (F1').

The ageing behavior in full cells of these three most promising formulations was studied in this paper. Although it can be considered that the three formulations are quite similar since they are all composed of 95% NMC532, significant differences are observed in their performance, whether

initially or after long-term cycling. Such discrepancies stem from the use of different binders (CMC/latex vs PVDF), current collectors (C-C Al vs bare aluminum), and even active material (considering that the NMC532 particle surface is not the same after immersion in NMP, water, or acidified water[20]—the NMC powders exposed to NMP, water, and acidified water will be denoted as P0, P1 and P2, respectively). In order to differentiate the influence of each of these parameters on the electrochemical performance in full cells, we will consider the F0, F1, F2-c, F1' and F2'c cathode formulations plus two other formulations, $P1_{NMP}$ and $P2_{NMP}$, which were introduced in a previous article[20]; the latter correspond to NMP-based electrodes (F0 type formulation) but they are prepared with NMC532 powder that had been exposed to water ($P1_{NMP}$) or acidified water ($P2_{NMP}$).

4.1 Influence of the aqueous processing on the NMC532 material

In order to study only the effect of the active material modification upon immersion in aqueous slurries, electrodes $P1_{NMP}$ and $P2_{NMP}$ were prepared, and their electrochemical performance was compared to $P0_{NMP}$ (here it corresponds to F0). A similar trend is found in the capacity decay between the NMP-based electrodes $P1_{NMP}$ and $P2_{NMP}$ and the water-based electrodes F1 and F2-c: although the initial capacity of the H_3PO_4-containing formulations ($P2_{NMP}$, F2-c) is generally lower than that of the acid-free formulations ($P1_{NMP}$, F1), the former exhibit better capacity retention so that they eventually outperform the latter (see **Figure S17**). This result indicates that the active material, more than the binder, influences the capacity retention of water-based electrodes. Besides, it also points out that aluminum corrosion is not the primary cause of capacity fading in the acid-free water-based formulations—it is rather related to the surface degradation of NMC532 in water—since even the corrosion-free electrode $P1_{NMP}$ exhibited faster capacity decay than $P0_{NMP}$ (i.e. F0).

How does the surface modification of the active material upon aqueous processing affect the cell electrochemical performance? In the acid-free formulation F1', the capacity fade mechanism was associated to performance degradation of the graphite anode (i.e. impedance buildup, see **Figure 4**, and poor HLD, see **Figure S7** and text below). It is suggested that, as the NMC532 material exposed to water (powder P1) contains more LiOH and adsorbed water (see **Figure S18**) than the one processed in acidified water (P2), a higher amount of HF is formed upon contact of the electrolyte[49,50] in the cells containing F1' electrodes. HF is known to attack the active material and dissolve TM ions[50,51]. As migration of TM ions—especially manganese—to the anode has been shown to increase lithium trapping in the graphite SEI[38,52], this mechanism is proposed to account for the performance degradation of graphite anode facing non-acidified water-based formulation F1'. Besides, the apparent decrease in the charge transfer resistance (**Figure 4**) and CEI thickness (**Table 3**) of F2-c cathode after ageing supports the idea that phosphate compounds formed on the NMC532 material during aqueous processing mitigate such TM dissolution and electrolyte decomposition.

4.2 Influence of the binder

The influence of the binder on the rate capability of NMC532 electrode has been evoked in section **3.2.2**. The use of PVDF or CMC/latex results in a different repartition of the carbon/polymer phase (see **Figure S9**), which impacts the rate performance. When CMC/latex is used, the carbon/CMC/latex mixture seems homogeneously distributed at the surface of the NMC particles, while the carbon/PVdF one is rather localized in the interstice between the NMC particles. The NMC coverage with carbon/CMC/latex phase appears to hinder fast lithium transfer in and out the active material particles as lower capacities are achieved at high C-rate with water-based electrodes. Incidentally, the reaction of electrolyte at the surface of NMC particles upon

ageing might be mitigated in the water-based electrodes compared to the electrode F0 containing PVDF, as in the latter, a higher NMC surface area is exposed to the electrolyte. The oxidative electrolyte decomposition—if indeed more significant in case of PVDF-based electrodes—would contribute, in F0, to the growth of the CEI layer (as observed by XPS, **Figure 5**), and of the charge transfer resistance (**Figure 4**) through surface structural transformation into less conductive spinel and even cubic phase.

Moreover, the lower capacity retention of F0 compared to F1' and F2-c after long-term cycling (see **Figure 2.b**) might also be related to the electrical degradation of the PVDF/carbon domains. Indeed, this capacity decay is associated to an increase of the cathode electronic and charge transfer resistances (R_2 and R_3, see **Figure 4**). Grillet et al.[36] have shown a correlation between mechanical stress of the PVDF/carbon mixture (occurring during cycling owing to successive lithium intercalation and extraction in LCO electrodes) and conductivity degradation in the cathode. According to the authors, since the PVdF/carbon mixture is much more electronically conductive than the cathode material, loss of adhesion of the PVdF/carbon domains at the interface with the NMC active material and/or loss of cohesion within the PVdF/carbon domains impact in turn the cathode, which results in the increase of the cell internal resistance (as it was observed in this study, **Figure S12**). Grissa et al.[41] also reported the degradation of PVDF binder upon mechanical stress, during the calendaring step. The authors observed through XPS analysis the presence of LiF at the surface of calendared NMC/PVDF electrodes, prior to contact with the electrolyte. As higher amount of LiF was found on heavily calendared electrodes, it was proposed that this compound originated from the reaction of fluorine from PVDF—upon mechanical stress—with lithium from NMC. A higher capacity fade was then observed for the electrodes with higher PVDF degradation. In this study, it is proposed that the degradation of the PVdF/carbon adhesion or cohesion upon

cycling contributes to the capacity decay observed with the formulation F0 due to the impedance rise at the cathode.

4.3 Influence of the carbon-coated collector

The carbon coating applied on aluminum collector can effectively prevent corrosion of the latter upon casting of water-based slurries, hence the capacity enhancement of F1' (C-C Al) compared to F1 (bare Al), as observed on half and full cells (see **Figure 1.a** and **Figure S10.a**). In particular, aluminum corrosion at the cathode seems to have a detrimental impact on the graphite anode, which exhibited the poorest HLD after long-term cycling (see **Figure S11**).

The use of C-C Al collector with F2 formulations (containing H_3PO_4) was also studied, to see if both strategies could combine into an improved formulation. Surprisingly however, such effect was not observed. On the contrary, when F2 slurries were coated onto C-C Al collector, the electrodes exhibited lower capacity retention than when the slurries were coated onto bare aluminum, whether they were cycled in half or full cells (see **Figure S5.a** and **Figure S10.b**). At this point it is not clear why seemingly worse performance is obtained with C-C Al compared to bare aluminum. Indeed, no single ageing mechanism seems to be at the origin of the capacity decay of water-based electrodes F1 and F2 coated on C-C Al collector, as different ageing behaviors were observed depending on the amount of phosphoric acid or anode used. In half cells, the electrodes F2'-a and F2'-b—containing respectively 0.1% and 0.3% H_3PO_4—exhibited a faster polarization growth when coated on C-C Al instead of bare aluminum (F2-a and F2-b), while for the electrode F2'-c and F2-c (0.5% H_3PO_4), no increased polarization was observed between the two collectors, only faster capacity loss in case of C-C Al (**Figure S5**). In full cells, differential voltage analysis has shown that graphite lithiation was less homogeneous when cycled against F2'-c (C-C Al) cathode compared to F2-c (bare Al). Several hypotheses have been drawn regarding the effect of

the carbon-coating collector on the electrochemical performance of the F2 electrodes, but none of them account for all the observations made above. It was proposed that H_3PO_4 could react with the polymers in the carbon coating, but in this case, it would be expected that the discrepancy between the electrochemical performances of both collectors would be more impacted at higher H_3PO_4 content.

It has also been suggested that the coating layer on C-C Al collector might release some species in the electrolyte that would migrate at the anode, obstructing the pores of graphite. This would account for the lower capacity at high current (5C) and lower HLD of graphite for the cells containing the cathodes with C-C Al collector (see **Figure S10.c** and **Figure S11**). In conclusion, there might be several mechanisms that account for the electrochemical performance obtained with C-C Al collector in this study, and it would be worth carrying further analyses, such as investigating the interaction of the carbon coating with H_3PO_4 as well as with the electrolyte.

5 SUMMARY

The applied aim of this work was to demonstrate the optimization of aqueous formulations of NMC532 electrodes so that they yield comparable electrochemical performance to conventional electrodes prepared in NMP solvent. Several aqueous formulations were developed with the aim of addressing a side-issue arising from the use of water instead of NMP which is the corrosion of the aluminum current collector. For this purpose, small amounts of phosphoric acid were added to the aqueous formulations, and the slurries were cast on carbon-coated aluminum foil besides bare current collectors.

The electrochemical performance of the different aqueous electrode formulations were assessed in half cells. Enhanced capacity retention was obtained for the acid-free formulation when using

the carbon coated aluminum collector (formulation F1') instead of bare aluminum, which reveals some detrimental impact of aluminum corrosion on the cycling performance. Regarding the formulations containing different amount of phosphoric acid (0.1%, 0.3%, 0.5% and 1%), the best performance are achieved at 0.5% H_3PO_4 (formulation F2-c).

The ageing behavior after long-term cycling in full NMC/graphite cells was investigated for the formulations F1' and F2-c, and compared to the reference NMP-based formulation F0. After more than 1000 cycles of constant cycling (charge at 0.5C, discharge at 1C), the electrode F0 exhibited the poorest capacity retention that was associated with an impedance buildup at the cathode. Two mechanisms were proposed to account for the poorer performance of the electrode containing PVDF binder. First, the surface area of NMC particles in direct contact with the electrolyte is higher when PVDF is used instead of CMC/latex, as a result of the different binder/carbon distribution. This could lead to higher electrolyte decomposition reactions at the cathode F0 surface, which is correlated to an increase in the thickness of the cathode electrolyte interface (CEI) observed by XPS, and could promote oxygen evolution from the NMC material, resulting in phase transformations that raise the charge transfer resistance. Besides, mechanical stress on PVDF/carbon domains upon cycling could cause loss of adhesion with NMC particles surface, or loss of cohesion within the PVDF/carbon domains, which would also result in increased impedance. Regarding the two water-based electrodes, faster capacity decay was observed with F1' compared to F2-c, which was correlated to performance degradation of the graphite anode. It was suggested that the higher LiOH and residual water content found on this electrode would react with the electrolyte to form HF that attacks the positive active material. Dissolved transition metals might migrate at the graphite anode and aggravate lithium consumption in the solid electrolyte interface. In contrast, the good capacity retention of the water-based electrode F2-c containing

0.5% H_3PO_4 might originate from the phosphate compounds formed at its surface following the electrode processing. It is suggested that these compounds protect the material from the electrolyte decomposition, as supported by the XPS analysis of CEI layer, as well as from dissolution. This study suggests that replacing NMP with water in the formulation of NMC532 electrodes can be done without sacrificing the electrochemical performance, although small modifications in the process can have big impact on the ageing behavior of the full cell. It points out also that prevention of the detrimental surface reactions of the NMC compound is mandatory.

ACKNOWLEDGEMENTS

This work was supported by the French Atomic and Alternative Energies Commission (CEA).

REFERENCES

1. Bresser, D., Buchholz, D., Moretti, A., Varzi, A. & Passerini, S. Alternative binders for sustainable electrochemical energy storage – the transition to aqueous electrode processing and bio-derived polymers. *Energy Environ. Sci.* **11**, 3096–3127 (2018).
2. Wood, D. L. *et al.* Technical and economic analysis of solvent-based lithium-ion electrode drying with water and NMP. *Dry. Technol.* **36**, 234–244 (2018).
3. Zhang, X. *et al.* Aging of LiNi1/3Mn1/3Co1/3O2 cathode material upon exposure to H2O. *J. Power Sources* **196**, 5102–5108 (2011).
4. Faenza, N. V. *et al.* Editors' Choice—Growth of Ambient Induced Surface Impurity Species on Layered Positive Electrode Materials and Impact on Electrochemical Performance. *J. Electrochem. Soc.* **164**, A3727–A3741 (2017).
5. Park, J., Park, J. & Lee, J. Stability of $LiNi_{0.6}Mn_{0.2}Co_{0.2}O_2$ as a Cathode Material for Lithium-Ion Batteries against Air and Moisture. *Bull. Korean Chem. Soc.* **37**, 344–348 (2016).

6. Shkrob, I. A. *et al.* Chemical Weathering of Layered Ni-Rich Oxide Electrode Materials: Evidence for Cation Exchange. *J. Electrochem. Soc.* **164**, A1489–A1498 (2017).
7. Liu, H., Yang, Y. & Zhang, J. Investigation and improvement on the storage property of LiNi0.8Co0.2O2 as a cathode material for lithium-ion batteries. *J. Power Sources* **162**, 644–650 (2006).
8. Sun, H.-H. & Manthiram, A. Impact of Microcrack Generation and Surface Degradation on a Nickel-Rich Layered Li[Ni $_{0.9}$ Co $_{0.05}$ Mn $_{0.05}$]O $_{2}$ Cathode for Lithium-Ion Batteries. *Chem. Mater.* **29**, 8486–8493 (2017).
9. Yang, Q., Wang, W., Qian, K. & Li, B. Investigation of Interfacial Changes on Grain Boundaries of Li(Ni $_{0.5}$ Co $_{0.2}$ Mn $_{0.3}$)O $_{2}$ in the Initial Overcharge Process. *Adv. Mater. Interfaces* **6**, 1801764 (2019).
10. Vetter, J. *et al.* Ageing mechanisms in lithium-ion batteries. *J. Power Sources* **147**, 269–281 (2005).
11. Jung, R. *et al.* Effect of Ambient Storage on the Degradation of Ni-Rich Positive Electrode Materials (NMC811) for Li-Ion Batteries. *J. Electrochem. Soc.* **165**, A132–A141 (2018).
12. Bauer, W., Çetinel, F. A., Müller, M. & Kaufmann, U. Effects of pH control by acid addition at the aqueous processing of cathodes for lithium ion batteries. *Electrochimica Acta* **317**, 112–119 (2019).
13. Memm, M., Hoffmann, A. & Wohlfahrt-Mehrens, M. Water-based LiNi1/3Mn1/3Co1/3O2-cathodes with good electrochemical performance by use of additives. *Electrochimica Acta* **260**, 664–673 (2018).
14. Li, S. Y. & Church, B. C. Effect of aqueous-based cathode slurry pH and immersion time on corrosion of aluminum current collector in lithium-ion batteries. *Mater. Corros.* **67**, 978–987 (2016).
15. Doberdo, I. *et al.* Enabling aqueous binders for lithium battery cathodes - Carbon coating of aluminum current collector. *J. Power Sources* **248**, 1000–1006 (2014).
16. Doberdò, I. *et al.* Enabling aqueous binders for lithium battery cathodes – Carbon coating of aluminum current collector. *J. Power Sources* **248**, 1000–1006 (2014).
17. Loeffler, N. *et al.* Performance of LiNi1/3Mn1/3Co1/3O2/graphite batteries based on aqueous binder. *J. Power Sources* **248**, 915–922 (2014).

18. Loeffler, N. *et al.* In Situ Coating of Li[Ni $_{0.33}$ Mn $_{0.33}$ Co $_{0.33}$]O $_{2}$ Particles to Enable Aqueous Electrode Processing. *ChemSusChem* **9**, 1112–1117 (2016).

19. Kuenzel, M. *et al.* Complementary Strategies Toward the Aqueous Processing of High-Voltage LiNi $_{0.5}$ Mn $_{1.5}$ O $_{4}$ Lithium-Ion Cathodes. *ChemSusChem* **11**, 562–573 (2018).

20. Bichon, M. *et al.* Study of Immersion of LiNi $_{0.5}$ Mn $_{0.3}$ Co $_{0.2}$ O $_{2}$ Material in Water for Aqueous Processing of Positive Electrode for Li-Ion Batteries. *ACS Appl. Mater. Interfaces* **11**, 18331–18341 (2019).

21. Gilbert, J. A. *et al.* Cycling behavior of NCM523/graphite lithium-ion cells in the 3–4.4 V range: Diagnostic studies of full cells and harvested electrodes. *J. Electrochem. Soc.* **164**, A6054–A6065 (2017).

22. Du, Z. *et al.* Enabling aqueous processing for crack-free thick electrodes. *J. Power Sources* **354**, 200–206 (2017).

23. Du, Z. *et al.* Three-dimensional conductive network formed by carbon nanotubes in aqueous processed NMC electrode. *Electrochimica Acta* **270**, 54–61 (2018).

24. Besnard, N. *et al.* Multiscale Morphological and Electrical Characterization of Charge Transport Limitations to the Power Performance of Positive Electrode Blends for Lithium-Ion Batteries. *Adv. Energy Mater.* **7**, 1602239 (2017).

25. Mao, C., Ruther, R. E., Li, J., Du, Z. & Belharouak, I. Identifying the limiting electrode in lithium ion batteries for extreme fast charging. *Electrochem. Commun.* **97**, 37–41 (2018).

26. Wood, M. *et al.* Chemical stability and long-term cell performance of low-cobalt, Ni-Rich cathodes prepared by aqueous processing for high-energy Li-Ion batteries. *Energy Storage Mater.* S2405829719309353 (2019) doi:10.1016/j.ensm.2019.08.020.

27. Jo, C.-H. *et al.* An effective method to reduce residual lithium compounds on Ni-rich Li[Ni0.6Co0.2Mn0.2]O2 active material using a phosphoric acid derived Li3PO4 nanolayer. *Nano Res.* **8**, 1464–1479 (2015).
28. Sahni, K. *et al.* H3PO4 treatment to enhance the electrochemical properties of Li(Ni1/3Mn1/3Co1/3)O2 and Li(Ni0.5Mn0.3Co0.2)O2 cathodes. *Electrochimica Acta* **301**, 8–22 (2019).
29. Lewerenz, M., Dechent, P. & Sauer, D. U. Investigation of capacity recovery during rest period at different states-of-charge after cycle life test for prismatic Li(Ni1/3Mn1/3Co1/3)O2-graphite cells. *J. Energy Storage* **21**, 680–690 (2019).
30. Loghavi, M. M., Askari, M., Babaiee, M. & Ghasemi, A. Improvement of the cyclability of Li-ion battery cathode using a chemical-modified current collector. *J. Electroanal. Chem.* **841**, 107–110 (2019).
31. Song, J. Two- and three-electrode impedance spectroscopy of lithium-ion batteries. *J. Power Sources* **111**, 255–267 (2002).
32. Levi, M. D. *et al.* Solid-State Electrochemical Kinetics of Li-Ion Intercalation into Li1ΧxCoO2: Simultaneous Application of Electroanalytical Techniques SSCV, PITT, and EIS. *J. Electrochem. Soc.* 11 (1999).
33. Zolin, L., Chandesris, M., Porcher, W. & Lestriez, B. An Innovative Process for Ultra-Thick Electrodes Elaboration: Toward Low-Cost and High-Energy Batteries. *Energy Technol.* **7**, 1900025 (2019).
34. Busson, C. *et al.* A primed current collector for high performance carbon-coated LiFePO4 electrodes with no carbon additive. *J. Power Sources* **406**, 7–17 (2018).
35. Ender, M., Illig, J. & Ivers-Tiffée, E. Three-Electrode Setups for Lithium-Ion Batteries: I. Fem-Simulation of Different Reference Electrode Designs and Their Implications for Half-Cell Impedance Spectra. *J. Electrochem. Soc.* **164**, A71–A79 (2017).

36. Grillet, A. M. *et al.* Conductivity Degradation of Polyvinylidene Fluoride Composite Binder during Cycling: Measurements and Simulations for Lithium-Ion Batteries. *J. Electrochem. Soc.* **163**, A1859–A1871 (2016).

37. Lewerenz, M., Fuchs, G., Becker, L. & Sauer, D. U. Irreversible calendar aging and quantification of the reversible capacity loss caused by anode overhang. *J. Energy Storage* **18**, 149–159 (2018).

38. Gilbert, J. A., Shkrob, I. A. & Abraham, D. P. Transition Metal Dissolution, Ion Migration, Electrocatalytic Reduction and Capacity Loss in Lithium-Ion Full Cells. *J. Electrochem. Soc.* **164**, A389–A399 (2017).

39. Harlow, J. E. *et al.* A Wide Range of Testing Results on an Excellent Lithium-Ion Cell Chemistry to be used as Benchmarks for New Battery Technologies. *J. Electrochem. Soc.* **166**, A3031–A3044 (2019).

40. Verdier, S. *et al.* XPS Study on Al2O3- and AlPO4-Coated LiCoO2 Cathode Material for High-Capacity Li Ion Batteries. *J. Electrochem. Soc.* **154**, A1088–A1099 (2007).

41. Grissa, R. *et al.* Thermomechanical Polymer Binder Reactivity with Positive Active Materials for Li Metal Polymer and Li-Ion Batteries: An XPS and XPS Imaging Study. *ACS Appl. Mater. Interfaces* **11**, 18368–18376 (2019).

42. Madec, L. *et al.* Understanding the Role of Prop-1-ene-1,3-Sultone and Vinylene Carbonate in LiNi0.3Mn0.3Co0.3O2-Graphite Pouch Cells: Electrochemical, GC-MS and XPS Analysis. *J. Electrochem. Soc.* **162**, A2635–A2645 (2015).

43. Yabuuchi, N., Kinoshita, Y., Misaki, K., Matsuyama, T. & Komaba, S. Electrochemical Properties of LiCoO2 Electrodes with Latex Binders on High-Voltage Exposure. *J. Electrochem. Soc.* **162**, A538–A544 (2015).

44. Jeschull, F. *et al.* Solid Electrolyte Interphase (SEI) of Water-Processed Graphite Electrodes Examined in a 65 mAh Full Cell Configuration. *ACS Appl. Energy Mater.* acsaem.8b00608 (2018) doi:10.1021/acsaem.8b00608.

45. Kuenzel, M. *et al.* Complementary Strategies Toward the Aqueous Processing of High-Voltage $LiNi_{0.5}Mn_{1.5}O_4$ Lithium-Ion Cathodes. *ChemSusChem* **11**, 562–573 (2018).
46. Nazri, G. Preparation, Characterization and Conductivity of Li3N, Li3P and Li3As. *MRS Proc.* **135**, 117 (1988).
47. Nazri, G. Preparation, structure and ionic conductivity of lithium phosphide. *Solid State Ion.* **34**, 97–102 (1989).
48. Reinhold, R. *et al.* Surface and Electrochemical Studies on Silicon Diphosphide as Easy-to-Handle Anode Material for Lithium-Based Batteries—the Phosphorus Path. *ACS Appl. Mater. Interfaces* **10**, 7096–7106 (2018).
49. Cui, X. *et al.* Influences of trace water on electrochemical performances for lithium hexafluoro phosphate- and lithium Bis(oxalato)borate-based electrolytes. *Electrochimica Acta* **273**, 191–199 (2018).
50. Xiong, X. *et al.* Washing effects on electrochemical performance and storage characteristics of LiNi0.8Co0.1Mn0.1O2 as cathode material for lithium-ion batteries. *J. Power Sources* **222**, 318–325 (2013).
51. Myung, S.-T. *et al.* Role of Alumina Coating on Li−Ni−Co−Mn−O Particles as Positive Electrode Material for Lithium-Ion Batteries. *Chem. Mater.* **17**, 3695–3704 (2005).
52. Shkrob, I. A. *et al.* Manganese in Graphite Anode and Capacity Fade in Li Ion Batteries. *J. Phys. Chem. C* **118**, 24335–24348 (2014).